PAPER

NCIRF: an organ dose calculator for patients undergoing radiography and fluoroscopy

Biomedical Physics & Engineering Express

PAPER

NCIRF: an organ dose calculator for patients undergoing radiography and fluoroscopy

Choonsik Lee[1,*], **Yeon Soo Yeom**[2,*], **Jungwook Shin**[1], **Seth W Streitmatter**[3] **and Cari M Kitahara**[1]

[1] Division of Cancer Epidemiology and Genetics, National Cancer Institute, National Institutes of Health, Rockville, MD, United States of America
[2] Department of Radiation Convergence Engineering, Yonsei University, Wonju, Republic of Korea
[3] Medical Imaging Physics and Radiation Safety, Department of Radiology and Imaging Sciences, University of Utah Health, Salt Lake City, UT, United States of America
[*] Authors to whom any correspondence should be addressed.

E-mail: choonsik.lee@nih.gov **and** ysyeom@yonsei.ac.kr

RECEIVED
7 December 2022

REVISED
25 April 2023

ACCEPTED FOR PUBLICATION
5 May 2023

PUBLISHED
23 May 2023

Keywords: organ, dose, fluoroscopy, patients, national cancer institute dosimetry system for radiography and fluoroscopy, radiography

Abstract

Background. It is critical to monitor the radiation dose delivered to patients undergoing radiography and fluoroscopy to prevent both acute and potential long-term adverse health effects. Accurate estimation of organ doses is essential to ensuring that radiation dose is maintained As Low As Reasonably Achievable. We developed a graphical user interface-based organ dose calculation tool for pediatric and adult patients undergoing radiography and fluoroscopy examinations. *Methods*. Our dose calculator follows the four sequential steps. First, the calculator obtains input parameters related to patient age and gender, and x-ray source data. Second, the program creates an input file describing the anatomy and material composition of a phantom, x-ray source, and organ dose scorers for Monte Carlo radiation transport using the user input parameters. Third, a built-in Geant4 module was developed to import the input file and to calculate organ absorbed doses and skeletal fluences through Monte Carlo radiation transport. Lastly, active marrow and endosteum doses are derived from the skeletal fluences and effective dose is calculated from the organ and tissue doses. Following benchmarking with MCNP6, we conducted some benchmarking calculations calculated organ doses for an illustrative cardeiac interventional fluoroscopy and compared the results with those from an existing dose calculator, PCXMC. *Results*. The graphical user interface-based program was entitled National Cancer Institute dosimetry system for Radiography and Fluoroscopy (NCIRF). Organ doses calculated from NCIRF showed an excellent agreement with those from MCNP6 in the simulation of an illustrative fluoroscopy exam. In the cardiac interventional fluoroscopy exam of the adult male and female phantoms, the lungs received relatively greater doses than any other organs. PCXMC based on stylistic phantoms overall overestimated major organ doses calculated from NCIRF by up to 3.7-fold (active bone marrow). *Conclusion*. We developed an organ dose calculation tool for pediatric and adult patients undergoing radiography and fluoroscopy examinations. NCIRF could substantially increase the accuracy and efficiency of organ dose estimation in radiography and fluoroscopy exams.

1. Introduction

The National Council on Radiation Protection and Measurements (NCRP) reported that radiography and fluoroscopy exams account for more than 20% of the mean annual individual effective dose from medical radiation sources in the United States (2.2 mSv in 2016) (NCRP 2019). It is critical to monitor the radiation dose delivered to patients undergoing radiography and fluoroscopy to prevent both acute and potential long-term adverse health effects. Accurate estimation of organ doses is essential to ensuring that radiation dose is maintained As Low As Reasonably Achievable (Strauss and Kaste 2006).

There may be several approaches to calculating organ doses for patients undergoing radiography or fluoroscopy exams. Two most frequently used ones include a lookup table of pre-calculated organ doses

and on-the-fly Monte Carlo calculation. First, a large number of dose calculations can be performed for the possible combinations of phantoms, projection geometries, and x-ray beam characteristics to create a lookup table of organ doses. When users select one of the combinations, pre-calculated organ doses are displayed. CALDose_X (Kramer *et al* 2008) is a computer program based on this approach. The program provides 29 organ doses for 34 projections of 10 commonly performed x-ray exams but does not support projection angles other than anteroposterior, posteroanterior, right lateral, and left lateral. VirtualDose-IR is another program using the pre-calculated look-up-table approach (Huo *et al* 2019). The program can calculate organ doses for the normal weight phantoms ranging from 5-year-old to adult, overweight adult phantoms, and 3, 6, and 9-months pregnant women exposed to x-ray beams with different energy spectra in typical irradiation geometries. Although the look-up-table methods can quickly provide organ doses, it is almost impossible to pre-define all combinations of patient parameters (e.g., age, gender, and body size) and machine parameters (e.g., beam energy, angle, and collimation), especially in interventional fluoroscopy procedures. The second approach to estimating organ doses for radiography and fluoroscopy exams is to embed Monte Carlo radiation transport codes into graphical user interface programs for users to perform Monte Carlo simulations using user input parameters. PCXMC (Tapiovaara *et al* 2008) has a built-in Monte Carlo engine to calculate organ doses from radiography and fluoroscopy. However, the anatomical models built in the program are simplified stylized phantoms (Cristy 1980). To the best of our knowledge, no calculation tools are available which are based on the on-the-fly Monte Carlo transport algorithm as well as realistic patient anatomy models.

To fill the critical gaps, we developed a user-friendly program entitled National Cancer Institute dosimetry system for Radiography and Fluoroscopy (NCIRF) by using a series of computational human phantoms combined with a streamlined Geant4 (Allison *et al* 2016) Monte Carlo radiation transport code. Following benchmarking with MCNP6, a general purpose Monte Carlo code, we calculated illustrative organ doses for interventional cardiac fluoroscopy procedures and compared the results with PCXMC.

2. Materials and methods

Our dose calculator follows the four sequential steps. First, the calculator obtains input parameters related to patient age and gender, and x-ray source data. Second, the program creates an input file describing the anatomy and material composition of a phantom, x-ray source, and organ dose scorers for Monte Carlo radiation transport using the user input parameters. Third, a built-in Geant4 module was developed to import the input file and to perform Monte Carlo radiation transport to calculate organ absorbed doses and skeletal fluences. Lastly, active marrow and endosteum doses are derived from the skeletal fluences and effective dose is calculated from the organ and tissue absorbed doses. The four steps are performed through a graphical user interface-based program created by using a cross-platform application development tool, Xojo (Xojo, Inc., Austin, TX). Each step is summarized in figure 1 and described in detail below.

2.1. User input parameters

The following parameters are obtained from users to create Monte Carlo input files for organ dose calculations. First, patient age (newborn, 1, 5, 10, 15 years, and adult) and gender (male or female) are acquired to select a computational human phantom. Users can also select from two different arm positions: raised arms and lowered arms. Second, a series of x-ray source parameters are obtained: beam quality (kVp and half-value layer (HVL)), beam isocenter, source-to-isocenter distance, beam angles (Positioner Primary Angle (PPA) from −180 to 180 degrees and Positioner Secondary Angle (PSA) from −45 to 45 degree), and the width and height of beam field at isocenter. Beam direction can be selected from a list of predefined angles: antero-posterior (AP), PA, left anterior oblique (LAO) 25 degree, right anterior oblique (RAO) 25 degree, left posterior oblique (LPO) 25 degree, right posterior oblique (RPO) 25 degree, cranial (CRA) 30 degree, and caudal (CAU) 30 degree. For absolute organ dose calculation, dose-area-product (DAP) (Gy-cm^2) is required. Lastly, the number of Monte Carlo histories and threads for parallel processing are acquired to run Monte Carlo radiation transport in multithreading mode.

2.2. Monte Carlo simulation input files

Based on the input parameters, we designed our program to generate Monte Carlo radiation transport input files for a general-purpose Monte Carlo code, MCNP6. MCNP6 code is export controlled commercial software and was not appropriate for our purposes. Instead, Geant4, which is permitted to redistribute (https://geant4.org/license/license.html), was coded to import MCNP6 input files and implemented into our program. We also keep the input files in MCNP6 format for users who may want to run the input files using their own MCNP6 with parallel computing servers. Below are more details about the three components of MCNP6 input files: computational human phantoms, x-ray source definition, and organ and skeletal tallies.

2.2.1. Computational human phantoms

We adopted the computational human phantom series developed in collaboration between the University of Florida and the National Cancer Institute

(Lee *et al* 2010). The phantom series represents newborn, 1-, 5-, 10-, and 15-year-old, and adult males and females, of which whole body dimension and organ masses are matched to the values of the International Commission on Radiological Protection (ICRP) (ICRP 2002). The original phantoms have the arms lowered. A new series of phantoms were created with the arms raised to more accurately describe arm position in some radiography and fluoroscopy procedures. The arm structures, including the skin, muscle, adipose, and skeletons (humeri, ulnae, radii, wrist, and hand bones), were manually translated and rotated using Rhinoceros (Robert McNeel & Associates, Seattle, WA), 3D modeling program. The two sets of the hybrid phantoms with the arms lowered and raised in mesh format were voxelized using an in-house MATLAB (Mathworks, Natick, MA) code with the voxel resolution ranging from $0.1326 \times 0.1326 \times 0.1326$ cm^3 (newborn) to $0.3158 \times 0.3158 \times 0.4414$ cm^3 (adult male). The matrix size of the phantoms was between 5 (newborn) to 7 (adult male) million voxels. Two sets of arm-raised and arm-lowered voxel phantoms in binary format were converted into *Lattice Card* in ASCII format, which were compatible with MCNP6. A total of 24 lattice files (12 phantoms with two arm postures) were implemented into the organ dose calculator.

Age-dependent elemental composition and density data for the organs and tissues in the computational human phantom series were adopted from the ICRP Publication 89 (ICRP 2002). The elemental composition was implemented into *Material Card* for MCNP6 code and densities were included into *Cell Card*. Age-dependent elemental compositions for the cortical bones, spongiosa bones, and cartilage of a total of 35 skeletal sites were adopted from the International Commission on Radiation Units and Measurements (ICRU) Report 46 (ICRU 1992) and ICRP Publication 89 (ICRP 2002).

2.2.2. X-ray source definition

One of the pre-defined x-ray spectra with different HVL values is selected by a user and implemented into MCNP6 source definition. A total of 25 x-ray spectra and HVL combinations were included: 50 kVp (HVL 1.89, 2.80, 3.30, 3.75 mm), 60 kVp (HVL 2.25, 3.42 mm), 70 kVp (HVL 2.61, 4.05, 6.83 mm), 80 kVp (HVL 3.01, 4.61, 5.57, 6.38, 7.70 mm), 90 kVp (HVL 3.38, 5.18 mm), 100 kVp (HVL 3.75, 5.71 mm), 110 kVp (HVL 4.11, 6.18, 7.33, 8.23, 9.68 mm), and 120 kVp (HVL 4.53, 6.52 mm).

The location of x-ray point source is defined using the isocenter, source-to-isocenter distance, and beam angles: PPA and PSA. PPA (from −180 to 180) and PSA (from −45 to 45) defined in the spherical coordinates are converted into the cartesian coordinates. The rotation of the original X, Y, and Z axes in phi (azimuthal angle) direction was converted to X′, Y′, and Z′ axes, and then the rotation of X′, Y′, and Z′ axes in theta (polar angle) direction was converted to X″, Y″, and Z″ axes. The angle differences between X″, Y″ and Z″ and X, Y, and Z are used for the *Transformation Card* in MCNP6.

X-ray source defined as a point source was then shaped in a rectangular cone beam when passing through a collimator of which size was adjusted to match the height and width of the beam field measured at the isocenter plane. Instead of an explicit collimator geometry, we assigned the importance of zero to the collimator to kill x-ray particles when they go through the collimator volume. The collimator was positioned 10 cm away from the x-ray source. Only air was modelled between the x-ray source and computational phantoms. Attenuation due to patient support common in fluoroscopy (e.g., table and pad) can be accounted for by scaling the DAP by the transmission of the support. The DAP meter volume was positioned 20 cm away from the x-ray source to score air kerma.

2.2.3. Organ and skeleton tallies

We included the following organs into the dose calculations: brain, pituitary gland, lens, eyeballs, salivary glands, oral cavity, spinal cord, thyroid, esophagus, trachea, thymus, lungs, breast, heart wall, stomach wall, liver, gallbladder, adrenals, spleen, pancreas, kidney, small intestine, colon, rectosigmoid, urinary bladder, prostate/uterus, gonads, skin, muscle, red bone marrow, and endosteum. Doses to the two sides were mass-averaged for paired organs such as lenses, eyeballs, salivary glands, thyroid, lungs, breast, adrenals, kidneys, and gonads. Doses to the walls were calculated for walled organs such as heart, stomach, small intestine, colon, rectosigmoid, and urinary bladder. Fluence was scored to the spongiosa regions of the skeleton by bone site and multiplied by dose response functions (ICRP 2010, Johnson *et al* 2011) to calculate doses to red marrow and endosteum. To increase the calculation speed, we calculated kerma per a launched photon (mGy/photon) instead of absorbed dose. We assumed charged particle equilibrium for the energy range of interest (50–120 kVp) in radiography and fluoroscopy.

We calculated air kerma (mGy-cm^2/photon) in the DAP meter volume and used the value to derive organ dose conversion coefficients (mGy/mGy-cm^2), organ dose per photon (mGy/photon) normalized to DAP (mGy-cm^2/photon). The conversion coefficients were multiplied by user-defined DAP values to calculate exam-specific absolute organ doses.

2.2.4. Batch Manager

To facilitate the simulation of multiple exams and efficiently manage the input parameters, we developed a user interface, called Batch Manager. Users can send the list of parameters they input into the graphical user interface to Batch Manager. The parameters include patient ID, phantom library (1 = arms lowered, 2 = arms raised), age group (1 = newborn, 2 = 1 year,

3 = 5 years, 4 = 10 years, 5 = 15 years, and 6 = adult), gender (1 = female, 2 = male), x-ray spectrum (kVp), HVL (mm), source-to-isocenter distance (cm), field width (cm), field height (cm), DAP (Gy-cm2), PPA (degree), PSA (degree), isocenter X, isocenter Y, isocenter Z, Monte Carlo particle history, and number of thread. The parameter list can be saved into a comma-separated values (CSV) format and the saved files can be loaded back to Batch Manager.

2.3. Geant4 Monte Carlo engine

To develop a built-in Monte Carlo dose calculation engine, we employed a general-purpose Monte Carlo radiation transport toolkit, Geant4 (Allison *et al* 2016). The Geant4 toolkit has been developed, updated, and maintained by an international collaboration of scientists and software engineers. The Geant4 toolkit is distributed as an open-source code (https://geant4.web.cern.ch/). The physics models of the Geant4 code have been intensively tested and validated with various experimental data and benchmarked with other Monte Carlo codes. As briefly described above, we developed a Geant4 routine to import MCNP6 main input and phantom lattice files. To simulate the voxelized geometry of the phantom, we used G4NestedParameterization class, optimized to the voxel navigation in the Geant4 code (Schümann *et al* 2012). To simulate the x-ray source, its position, direction, and energy spectra were defined by using the G4VUserPrimaryGeneratorAction class.

We streamlined the size of the Geant4 package by excluding *Visualization, Persistency, Interfaces, Intercoms*, and part of *Tracking Modules*. We only included the cross section/physics data required for photon transport (G4EMLOW and G4ENSDFSTATE). To simulate the Compton scattering interaction, G4KleinNishinaModel was applied while G4LivermorePhotoElectricModel was applied to simulate the photoelectric absorption. The default value for secondary range cut was set for photons but was increased to a long value (e.g., 1 km) not to transport secondary electrons. Two Geant4 execution files with multithreading capability were created for Mac and Windows and included into the organ dose calculator. The final size of the streamlined Geant4 package was about 40 MB.

2.4. Calculation of active marrow and effective dose

We adopted the skeletal dose response function (ICRP 2010, Johnson *et al* 2011) to calculate active marrow and endosteum doses. The dose response function is composed of two sets of conversion factors, which convert the fluence scored to the spongiosa region underneath the cortical layer to absorbed doses to active marrow and endosteum within the given bone site, respectively. Bone site-specific doses are then weighted by the fraction of active marrow and endosteum contained in each bone site to derive the whole body active marrow and endosteum doses.

We employed the tissue weighting factors published in ICRP Publication 103 (ICRP 2007) to derive effective doses from organ and tissue doses. The complete definition of effective dose requires the average of the male- and female-specific organ doses such as the testes and prostate for males and the ovaries and uterus for females. Since a single gender phantom is involved in a simulation, we only derived a gender-specific effective dose.

2.5. Performance evaluation

We conducted four types of performance evaluations. The same simulation scenario was used for all tests: left-anterior-oblique (LAO) projection with PPA of 25 degree and PSA of −25 degree on the adult male phantom using the x-ray beam with 70 kVp, 6.83 mm Al HVL and the field size of 19 × 19 cm^2. First, we calculated the organ doses normalized to DAP (mGy/Gy-cm^2) using our calculator (based on Geant4) and compared the results with those calculated from MCNP6. Doses to major organs in the chest and abdomen regions were compared: spinal cord, thyroid, esophagus, trachea, thymus, lungs, breast, heart wall, stomach wall, liver, gallbladder, adrenals, spleen, pancreas, and kidney. To prevent misleading discrepancies caused by Monte Carlo errors, we conducted five repetitions of each calculation and then compared the mean organ doses bewteen the two Monte Carlo codes. Second, dose calculation time (min) was measured for an increasing number of threads ranging from 1 to 18 to evaluate the impact of multithreading on calculation time. We used an iMac Pro 18-core Intel 2.3 GHz Xeon W for the test and ran 10^7 Monte Carlo histories. Third, we measured Monte Carlo relative error (%) for increasing particle history ranging from 10^4 to 10^8 to evaluate how increasing particle history reduces Monte Carlo errors. We calculated organ dose per DAP for the heart wall (in-field), lungs (in-field), and thyroid (out-of-field).

Finally, we tested the impact of the arm position on organ doses by simulating right and left lateral projections for the arm-raised and arm-lowered adult male phantoms. We used a 70 kVp, 6.83 mm Al HVL x-ray beam with a field size of 19 × 19 cm^2. Doses to the esophagus, lungs, breast, heart wall, and liver were compared.

After the performance evaluations, we calculated illustrative organ doses for adult male and female phantoms undergoing a cardiac interventional fluoroscopy procedure with five common beam projections. The parameters used for the simulations are tabulated in table 1. We also simulated the identical (as much as possible) projections using an existing organ dose calculator, PCXMC (Tapiovaara *et al* 2008), and compared its organ doses with those from our dose calculator. For fair comparison, it was confirmed that our x-ray spectrum was in good agreement with those extracted from PCXMC. Since PCXMC only provides

Table 1. Patient and technical parameters used for simulating cardiac fluoroscopy projection procedures: phantom library (1 = arms lowered, 2 = arms raised), age group (1 = newborn, 2 = 1 year, 3 = 5 years, 4 = 10 years, 5 = 15 years, and 6 = adult), gender (1 = female, 2 = male), half value layer (HVL); source-to-isocenter distance (SID); field width (W) and height (H); positioner primary angle (PPA); positioner secondary angle (PSA).

Patient ID	Phantom library	Age group	Gender	x-ray energy (kV)	HVL (mm)	SID (cm)	Field W (cm)	Field H (cm)	DAP (Gy-cm^2)	PPA (degree)	PSA (degree)	Iso Ctr X (cm)	Iso Ctr Y (cm)	Iso Ctr Z (cm)	History	Threads
10 001	2	6	2	70	6.83	63.5	19	19	1	0	0	32.8	29.9	133.5	10 000 000	10
10 002	2	6	1	70	6.83	63.5	19	19	1	0	0	28.5	28.8	125.3	10 000 000	10
10 003	2	6	2	70	6.83	63.5	19	19	1	25	−25	32.8	29.9	133.5	10 000 000	10
10 004	2	6	2	70	6.83	63.5	19	19	1	25	25	32.8	29.9	133.5	10 000 000	10
10 005	2	6	2	70	6.83	63.5	19	19	1	−25	−25	32.8	29.9	133.5	10 000 000	10
10 006	2	6	2	70	6.83	63.5	19	19	1	−25	25	32.8	29.9	133.5	10 000 000	10
10 007	2	6	1	70	6.83	63.5	19	19	1	25	−25	28.5	28.8	125.3	10 000 000	10
10 008	2	6	1	70	6.83	63.5	19	19	1	25	25	28.5	28.8	125.3	10 000 000	10
10 009	2	6	1	70	6.83	63.5	19	19	1	−25	−25	28.5	28.8	125.3	10 000 000	10
10010	2	6	1	70	6.83	63.5	19	19	1	−25	25	28.5	28.8	125.3	10000000	10

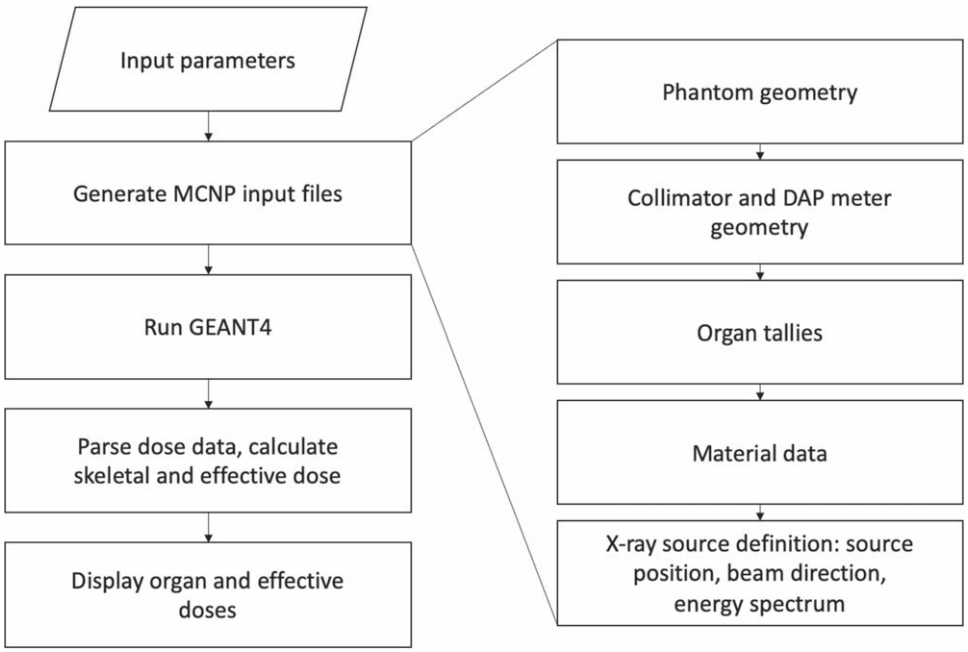

Figure 1. Flowchart of National Cancer Institute dosimetry system for Radiography and Fluoroscopy (NCIRF).

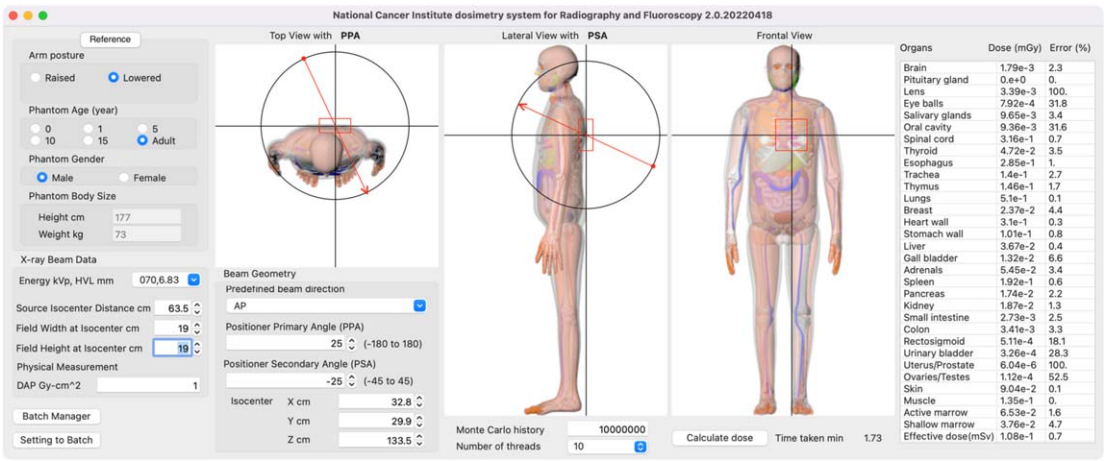

Figure 2. Graphical user interface of the National Cancer Institute dosimetry system for Radiography and Fluoroscopy (NCIRF) main window.

organ doses for a hermaphrodite stylized phantom, a single set of organ doses from PCXMC was compared with that of the adult male and female phantoms in our calculator.

3. Results

3.1. NCIRF

We titled the dose calculator as the National Cancer Institute dosimetry system for Radiography and Fluoroscopy (NCIRF). Figure 2 shows the graphical user interface of NCIRF where LAO 25 CAU 25 projection with 70 kVp 6.83 mm Al HVL and the field size 19 × 19 cm^2 was simulated for the adult male phantom with the arms lowered. Users can open Batch Manager by clicking the 'Batch Manager' button in the main program or 'Setting to Batch' button which will send the parameters to Batch Manager. Users can run multiple of Monte Carlo simulations using Batch Manager.

3.2. Performance evaluation

Organ doses calculated from Geant4 showed excellent agreement (< 3%) with those from MCNP6 in the simulation of an illustrative cardiac fluoroscopy exam (figure 3). Small organs such as the thyroid, thymus, breast, and adrenals show relatively greater discrepancies between 2% and 3% compared to other organs.

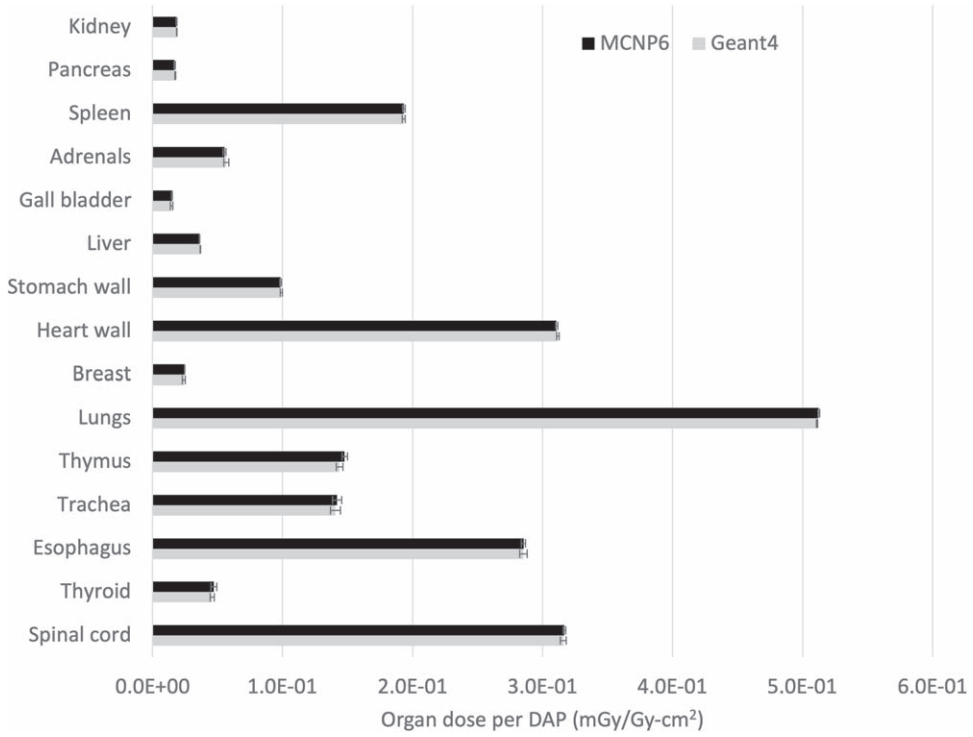

Figure 3. Comparison of major organ doses for a simple antero-posterior projection between NCIRF (Geant4) and MCNP6.

Calculation time exponentially decreased by increasing threads (figure 4(A)). When the number of threads increased from 1 to 3, calculation time decreased by about 63% (14.2 min to 5.2 min). When threads were increased threefold from 3 to 9, calculation time decreased by about 60% again (5.2 min to 2.1 min). However, the improvement in calculation time was only 43% (2.1 min to 1.2 min) when threads were doubled from 9 to 18.

The Monte Carlo errors exponentially decreased by increasing the number of Monte Carlo history (figure 4(B)). The error in the heart wall (in-field) decreased to 0.9% when the history of 10^6 was used. The error in the lungs (in-field) decreased to 0.4% when 10^6 particles were launched. The thyroid (out-of-field) showed the error of 13.2% after 10^6 particles were simulated and required 10^8 particle history to achieve the error close to 1%.

The liver and stomach of the adult male phantoms received 4.4 (RLAT) and 5.3 (LLAT) times greater doses when the arms were raised compared to when the arms lowered (table 2). The adrenals were the next organs showing the significant impact (ratio of 3.4) of the arms in the RLAT exam. In the LLAT exam, the liver, gallbladder, and spleen showed a similar ratio of 4.2. The average ratios in the RLAT and LLAT exams were 2.4 and 2.9, respectively.

3.3. Organ doses for cardiac interventional fluoroscopy

In the cardiac interventional fluoroscopy procedure of the adult male and female phantoms, the lungs received relatively greater average doses than other organs when DAP was set unity: 0.51 mGy (adult male, table 3(A)) and 0.58 mGy (adult female, table 3(B)). The spleen and esophagus also showed relatively high doses. Those high dose organs were followed by the heart wall which showed the dose ranging from 0.39 to 0.40 mGy. From the five projections, the lungs of the adult male and female phantoms received a total of 2.56 and 2.89 mGy, respectively. The total effective doses were 0.69 (male) and 0.78 (female) mSv.

The total heart wall dose from PCXMC (2.16 mGy) (table 3(C)) was slightly greater than those from NCIRF (1.95 mGy for male and 2.02 mGy for female). However, PCXMC overall over- or under-estimated the doses to the major critical organs. The total active marrow dose from PCXMC was 3.66 and 3.49 times greater than those of the adult male and female of NCIRF, respectively (table 4). The breast dose from PCXMC was also 2.48 (male) and 2.07 (female) times greater than those from NCIRF. In contrast, the thyroid and gallbladder doses from PCXMC was about 40% (male) and 20% (female) of those from NCIRF.

4. Discussion

NCIRF has several strengths compared to other existing tools. First, the realistic hybrid computational human phantoms were implemented for accurate dose calculations. Several studies revealed the anatomical limitation of the old stylized phantoms in external radiation dosimetry (Bellamy *et al* 2016, Dewji *et al* 2018, Borrego *et al* 2019, Griffin *et al* 2020). The realistic arm position in NCIRF showed

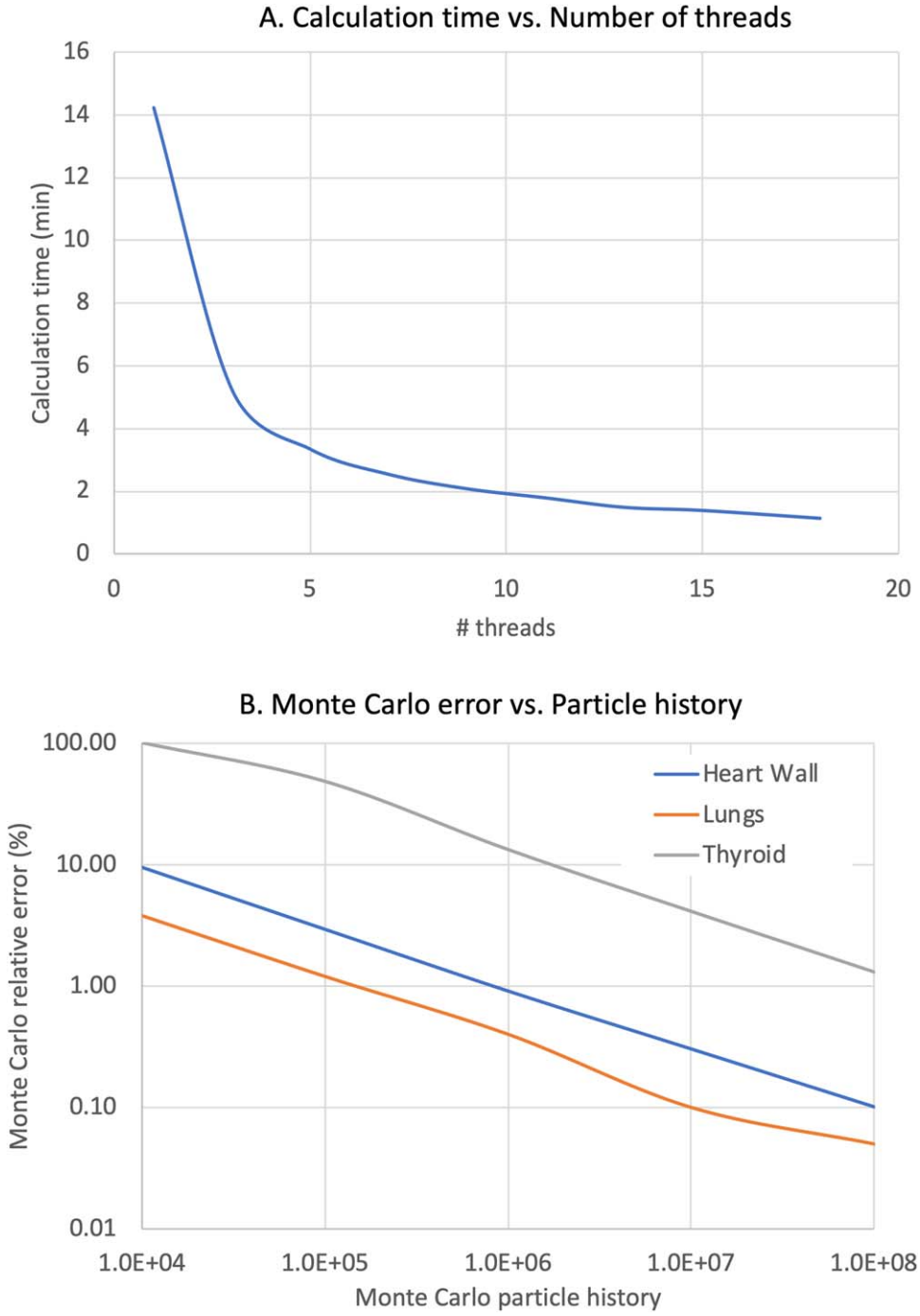

Figure 4. Impact of (a) the number of threads on calculation time and (b) Monte Carlo particle history on Monte Carlo relative errors.

substantial impact on internal organ doses in lateral x-ray exams. Active marrow dose calculation is based on the detailed skeleton models combined with the latest skeletal dose response function derived from micro CT-based Monte Carlo simulations (ICRP 2010, Johnson *et al* 2011). Second, organ dose calculation is performed using the on-the-fly Monte Carlo radiation transport based on the Geant4, which has been rigorously validated since its introduction in the 1990s. Significant improvement in calculation speed was achieved through the hyper-threading technique. Lastly, NCIRF provides several user-friendly and efficient features. The direction, size, and position of x-ray beams can be visually defined on a computational phantom. Batch Manager allows for calculating organ doses for multiple exams through a convenient interface to import and export many sets of patient and technical parameters.

We observed substantial differences in the doses to the organs surrounding the heart in cardiac interventional fluoroscopy procedures between NCIRF and PCXMC. The discrepancy may be caused by the

Table 2. Organ doses per unit dose-area-product (DAP) (mGy/Gy-cm^2) for the adult male phantoms with the arms lowered and raised in right lateral (RLAT) and left lateral (LLAT) exams. The x-ray beam with the energy of 70 kVp (6.83 mm HVL) and the field size 19 × 19 cm^2 was used for the simulations.

	Arms lowered		Arms raised		Raised/Lowered	
	RLAT	LLAT	RLAT	LLAT	RLAT	LLAT
Spinal cord	0.033	0.031	0.093	0.108	2.8	3.5
Thyroid	0.018	0.018	0.025	0.029	1.4	1.6
Esophagus	0.140	0.111	0.420	0.380	3.0	3.4
Trachea	0.079	0.068	0.114	0.095	1.4	1.4
Thymus	0.149	0.189	0.164	0.175	1.1	0.9
Lungs	0.441	0.331	0.904	0.782	2.1	2.4
Breast	0.148	0.138	0.214	0.216	1.4	1.6
Heart wall	0.247	0.563	0.553	1.168	2.2	2.1
Stomach wall	0.035	0.174	0.087	0.915	2.5	5.3
Liver	0.170	0.035	0.743	0.148	4.4	4.2
Gallbladder	0.042	0.017	0.122	0.073	2.9	4.2
Adrenals	0.032	0.040	0.108	0.161	3.4	4.0
Spleen	0.017	0.108	0.056	0.456	3.3	4.2
Pancreas	0.008	0.023	0.024	0.073	2.9	3.1
Kidney	0.011	0.012	0.032	0.042	3.0	3.4
Small intestine	0.004	0.004	0.011	0.010	2.8	2.9
Colon	0.007	0.007	0.014	0.017	2.1	2.5
Active marrow	0.052	0.049	0.105	0.099	2.0	2.0
Shallow marrow	0.030	0.028	0.058	0.055	2.0	2.0
Effective dose	0.102	0.101	0.218	0.287	2.1	2.8

anatomical difference between the realistic hybrid phantoms in NCIRF and the simplified stylized hermaphrodite phantoms in PCXMC. These findings agreed with those from a previous study (Park *et al* 2008) where a Monte Carlo simulation study of cardiac catheterization was conducted using stylized and voxel phantoms. They also reported organ dose discrepancies between the two phantom types caused by the unrealistic anatomy in the stylized phantoms.

We are aware of the following limitations in the current version of NCIRF. First, although we adopted a series of computational human phantoms matched to the reference anatomical data of ICRP, it should be noted that there are still anatomical differences between the phantoms and patients. Second, although we achieved reasonable improvement in calculation speed using hyper threading, the direct Monte Carlo radiation transport-based dose calculation is slower (minute to several minutes depending on threads) than the method based on pre-calculated dose tables (instantaneous to seconds). As stated in the introduction, however, it is important to make the calculation tool flexible and versatile to accurately account for various technical parameters including beam energy and angles, field size, source-to-isocentere distance, etc. Future studies may include the implementation of Graphical Processing Unit-based Monte Carlo calculation engines to speed up the radiation transport process. Third, the variation in body size or anatomical changes due to pregnancy were not accounted for in the current version of NCIRF. We plan to extend the phantom library to include the body size-dependent phantom library (Geyer *et al* 2014) and pregnant women phantoms (Maynard *et al* 2014) in the future. Lastly, a way to generate customized x-ray spectra, where the user defines the kVp and added filtration, is planned to be included as a future feature of NCIRF to offer even greater flexibility.

5. Conclusion

We developed a graphical user interface-based organ dose calculation tool, NCIRF, for pediatric and adult patients undergoing radiography and fluoroscopy examinations by using a series of realistic computational human phantoms combined with the Geant4 Monte Carlo package. Organ doses calculated from NCIRF showed an excellent agreement with those from MCNP6 in the simulation of an illustrative fluoroscopy exam. PCXMC based on stylistic phantoms overall overestimated major organ doses calculated from our program. NCIRF could substantially increase the accuracy and efficiency of organ dose estimation in radiography and fluoroscopy exams for pediatric and adult patients. The program should be useful to accurately monitor organ-level doses to ensure the delivered dose is As Low As Reasonably Achievable.

Table 3. Organ doses (mGy) and effective doses (mSv) for five fluoroscopy projections calculated from (A) NCIRF adult male phantom, (B)NCIRF adult female phantom, and (C) PCXMC hermaphrodite phantom.

A. NCIRF, Adult Male	PPA/PSA (degree)					Total	Average
	25/−25	25/25	−25/−25	−25/25	0/0		
Thyroid	0.046	0.015	0.120	0.018	0.036	0.235	0.047
Esophagus	0.293	0.285	0.415	0.389	0.505	1.887	0.377
Thymus	0.147	0.063	0.249	0.073	0.212	0.745	0.149
Lungs	0.511	0.399	0.613	0.437	0.602	2.562	0.512
Breast	0.026	0.035	0.027	0.045	0.069	0.202	0.040
Heart wall	0.312	0.302	0.414	0.359	0.564	1.951	0.390
Stomach wall	0.099	0.297	0.091	0.300	0.324	1.112	0.222
Liver	0.037	0.061	0.064	0.260	0.101	0.523	0.105
Gall bladder	0.015	0.034	0.023	0.169	0.037	0.278	0.056
Adrenals	0.058	0.275	0.063	0.495	0.116	1.006	0.201
Spleen	0.195	1.172	0.170	0.655	0.420	2.613	0.523
Pancreas	0.017	0.118	0.016	0.075	0.037	0.263	0.053
Kidney	0.019	0.099	0.019	0.102	0.035	0.275	0.055
Skin	0.090	0.107	0.085	0.091	0.077	0.451	0.090
Muscle	0.136	0.136	0.140	0.140	0.141	0.692	0.138
Active marrow	0.065	0.059	0.066	0.061	0.065	0.315	0.063
Effective dose (mSv)	0.109	0.133	0.131	0.150	0.169	0.691	0.138
B. NCIRF, Adult Female	PPA/PSA (degree)					Total	Average
	25/−25	25/25	−25/−25	−25/25	0/0		
Thyroid	0.090	0.032	0.217	0.038	0.079	0.456	0.091
Esophagus	0.363	0.370	0.520	0.494	0.652	2.400	0.480
Thymus	0.181	0.073	0.378	0.093	0.254	0.979	0.196
Lungs	0.524	0.432	0.670	0.515	0.749	2.891	0.578
Breast	0.027	0.039	0.033	0.046	0.096	0.242	0.048
Heart wall	0.295	0.291	0.443	0.385	0.600	2.015	0.403
Stomach wall	0.085	0.322	0.069	0.240	0.325	1.041	0.208
Liver	0.045	0.089	0.079	0.358	0.162	0.733	0.147
Gall bladder	0.035	0.086	0.048	0.303	0.099	0.571	0.114
Adrenals	0.047	0.266	0.050	0.777	0.106	1.246	0.249
Spleen	0.131	1.092	0.100	0.359	0.276	1.957	0.391
Pancreas	0.035	0.271	0.035	0.272	0.085	0.698	0.140
Kidney	0.025	0.165	0.026	0.211	0.051	0.479	0.096
Skin	0.108	0.121	0.096	0.099	0.085	0.508	0.102
Muscle	0.148	0.148	0.152	0.155	0.157	0.760	0.152
Active marrow	0.066	0.055	0.074	0.062	0.074	0.331	0.066
Effective dose (mSv)	0.114	0.148	0.147	0.167	0.202	0.778	0.156
C. PCXMC	PPA/PSA (degree)					Total	Average
	25/−25	25/25	−25/−25	−25/25	0/0		
Thyroid	0.009	0.019	0.027	0.012	0.023	0.091	0.018
Esophagus	0.406	0.441	0.454	0.460	0.486	2.246	0.449
Thymus	0.149	0.165	0.235	0.212	0.146	0.906	0.181
Lungs	0.566	0.570	0.719	0.702	0.621	3.179	0.636
Breast	0.077	0.083	0.125	0.097	0.119	0.501	0.100
Heart wall	0.349	0.315	0.567	0.522	0.408	2.161	0.432
Stomach wall	0.067	0.079	0.126	0.136	0.114	0.521	0.104
Liver	0.133	0.052	0.037	0.047	0.074	0.344	0.069
Gall bladder	0.031	0.011	0.023	0.022	0.024	0.112	0.022
Adrenals	1.304	0.118	0.574	0.130	0.127	2.254	0.451
Spleen	0.172	0.134	0.673	0.120	0.089	1.190	0.238
Pancreas	0.179	0.082	0.227	0.138	0.107	0.732	0.146
Kidney	0.098	0.020	0.074	0.020	0.020	0.232	0.046
Skin	0.087	0.085	0.083	0.080	0.080	0.415	0.083
Muscle	0.100	0.103	0.105	0.099	0.102	0.509	0.102
Active marrow	0.247	0.245	0.197	0.217	0.247	1.153	0.231

Table 4. Ratio of organ and effective doses per five different projections and total doses calculated from PCXMC to those from NCIRF adult male and female phantoms.

	Ratio PCXMC/NCIRF,M						Ratio PCXMC/NCIRF,F					
	25/−25	25/25	−25/−25	−25/25	0/0	Total	25/−25	25/25	−25/−25	−25/25	0/0	Total
Thyroid	0.20	1.22	0.23	0.68	0.64	0.39	0.10	0.59	0.13	0.32	0.29	0.20
Esophagus	1.38	1.55	1.10	1.18	0.96	1.19	1.12	1.19	0.87	0.93	0.74	0.94
Thymus	1.01	2.61	0.94	2.88	0.69	1.22	0.82	2.26	0.62	2.29	0.57	0.93
Lungs	1.11	1.43	1.17	1.61	1.03	1.24	1.08	1.32	1.07	1.36	0.83	1.10
Breast	2.98	2.37	4.63	2.14	1.74	2.48	2.85	2.12	3.74	2.10	1.24	2.07
Heart wall	1.12	1.04	1.37	1.46	0.72	1.11	1.18	1.08	1.28	1.36	0.68	1.07
Stomach wall	0.67	0.27	1.38	0.45	0.35	0.47	0.78	0.25	1.83	0.56	0.35	0.50
Liver	3.63	0.86	0.58	0.18	0.74	0.66	2.94	0.59	0.47	0.13	0.46	0.47
Gall bladder	2.08	0.34	1.00	0.13	0.65	0.40	0.91	0.13	0.47	0.07	0.25	0.20
Adrenals	22.48	0.43	9.16	0.26	1.10	2.24	27.89	0.44	11.44	0.17	1.20	1.81
Spleen	0.88	0.11	3.97	0.18	0.21	0.46	1.32	0.12	6.75	0.33	0.32	0.61
Pancreas	10.38	0.69	13.86	1.85	2.89	2.78	5.08	0.30	6.54	0.51	1.25	1.05
Kidney	5.24	0.20	3.79	0.20	0.57	0.84	3.85	0.12	2.80	0.10	0.39	0.48
Skin	0.96	0.79	0.97	0.88	1.04	0.92	0.81	0.71	0.86	0.81	0.94	0.82
Muscle	0.74	0.76	0.75	0.71	0.73	0.74	0.68	0.70	0.69	0.64	0.65	0.67
Active marrow	3.79	4.19	2.99	3.56	3.82	3.66	3.76	4.42	2.67	3.52	3.33	3.49
Effective dose(mSv)	1.51	1.15	1.45	1.18	1.01	1.24	1.44	1.03	1.29	1.06	0.85	1.10

Acknowledgment

This research was funded by the intramural research program of the National Institutes of Health, National Cancer Institute, Division of Cancer Epidemiology and Genetics.

Data availability statement

The data that support the findings of this study are openly available at the following URL: https://dceg.cancer.gov/tools/radiation-dosimetry-tools/radiography-fluoroscopy.

ORCID iDs

Choonsik Lee https://orcid.org/0000-0003-4289-9870
Yeon Soo Yeom https://orcid.org/0000-0001-5373-6693

References

Allison J *et al* 2016 Recent developments in Geant4 *Nucl. Instrum. Methods Phys. Res. Sect. Accel. Spectrometers Detect. Assoc. Equip.* **835** 186–225

Bellamy M B, Hiller M M, Dewji S A, Veinot K G, Leggett R W, Eckerman K F, Easterly C E and Hertel N E 2016 Comparison of monoenergetic photon organ dose rate coefficients for stylized and voxel phantoms submerged in air *Radiat. Prot. Dosimetry* **172** 367–74

Borrego D, Apostoaei A I, Thomas B A, Hoffman F O, Simon S L, Zablotska L B and Lee C 2019 Organ-specific dose coefficients derived from Monte Carlo simulations for historical (1930s to 1960s) fluoroscopic and radiographic examinations of tuberculosis patients *J. Radiol. Prot.* **39** 950–65

Cristy M 1980 *Mathematical Phantoms Representing Children Of Various Ages For Use In Estimates Of Internal Dose* (Oak Ridge, TN: Oak Ridge National Laboratory)

Dewji S A, Bales K, Griffin K, Lee C and Hiller M 2018 Age-dependent comparison of monoenergetic photon organ and effective dose coefficients for pediatric stylized and voxel phantoms submerged in air *Phys. Med. Biol.* **63** 175019

Geyer A M, O'Reilly S, Lee C, Long D J and Bolch W E 2014 The UF/NCI family of hybrid computational phantoms representing the current US population of male and female children, adolescents, and adults–application to CT dosimetry *Phys. Med. Biol.* **59** 5225–42

Griffin K T, Cuthbert T A, Dewji S A and Lee C 2020 Stylized versus voxel phantoms: a juxtaposition of organ depth distributions *Phys. Med. Biol.* **65** 065007

Huo W, Pi Y, Feng M, Qi Y, Gao Y, Caracappa P F, Chen Z and Xu X G 2019 VirtualDose-IR: a cloud-based software for reporting organ doses in interventional radiology *Phys. Med. Biol.* **64** 095012

ICRP 2002 Basic anatomical and physiological data for use in radiological protection : reference values *ICRP Publ. 89 Ann ICRP* **32** 1–277

ICRP 2007 The 2007 Recommendations of the international commission on radiological protection *ICRP Publ. 103 Ann ICRP* **37** 1–332

ICRP 2010 Conversion coefficients for radiological protection quantities for external radiation exposures *ICRP Publ. 116 Ann ICRP* **40** 1–258

ICRU 1992 Photon, electron, proton and neutron interaction data for body tissues *ICRU Rep. 46 J. ICRU* **os24** Online: (https://academic.oup.com/jicru/article/os24/1/NP/2923816)

Johnson P B, Bahadori A A, Eckerman K F, Lee C and Bolch W E 2011 Response functions for computing absorbed dose to skeletal tissues from photon irradiation - an update *Phys. Med. Biol.* **56** 2347

Kramer R, Khoury H J and Vieira J W 2008 CALDose_X—a software tool for the assessment of organ and tissue absorbed doses, effective dose and cancer risks in diagnostic radiology *Phys. Med. Biol.* **53** 6437–59

Lee C, Lodwick D, Hurtado J, Pafundi D, Williams J L and Bolch W E 2010 The UF family of reference hybrid phantoms for computational radiation dosimetry *Phys. Med. Biol.* **55** 339–63

Maynard M R, Long N S, Moawad N S, Shifrin R Y, Geyer A M, Fong G and Bolch W E 2014 The UF Family of hybrid phantoms of the pregnant female for computational radiation dosimetry *Phys. Med. Biol.* **59** 4325–43

NCRP 2019 *Medical Radiation Exposure of Patients in the United States* Online: (https://ncrponline.org/shop/reports/report-no-184-medical-radiation-exposure-of-patients-in-the-united-states-2019/)

Park S H, Lee J K and Lee C 2008 Dose conversion coefficients calculated using tomographic phantom, KTMAN-2, for X-ray examination of cardiac catheterisation *Radiat. Prot. Dosimetry* **128** 351–8 Online: (http://rpd.oxfordjournals.org/content/128/3/351.long)

Schümann J, Paganetti H, Shin J, Faddegon B and Perl J 2012 Efficient voxel navigation for proton therapy dose calculation in TOPAS and Geant4 *Phys. Med. Biol.* **57** 3281–93

Strauss K J and Kaste S C 2006 The ALARA (as low as reasonably achievable) concept in pediatric interventional and fluoroscopic imaging: striving to keep radiation doses as low as possible during fluoroscopy of pediatric patients–a white paper executive summary *Pediatr. Radiol.* **36** 110–2

Tapiovaara M, Lakkisto M and Servomaa A 2008 *PCXMC - A PC-Based Monte Carlo Program for Calculating Patient Doses in Medical X-ray Examinations* 2nd edn (Helsinki, Finland: Radiation and Nuclear Safety Authority (STUK))